

Highly stable nanostructured magnetic vesicles as doxorubicin carriers for field-assisted therapies

Heber E. Andrada^{*[a,b]}, Lisandro Venosta^[c,d], Silvia E. Jacobo^[e], O. Fernando Silva^[f], R. Darío Falcone^[a,b],

Paula G. Bercoff^{*[c,d]}

[a] Departamento de Química, Universidad Nacional de Río Cuarto, Córdoba, Argentina.

[b] Instituto de desarrollo Agroindustrial y de la Salud (IDAS), Universidad Nacional de Río Cuarto, Córdoba, Argentina.

[c] Instituto de Física Enrique Gaviola (IFEG), CONICET, Ciudad Universitaria, Córdoba, Argentina.

[d] Facultad de Matemática, Astronomía, Física y Computación (FAMAF), Universidad Nacional de Córdoba, Ciudad Universitaria, Córdoba, Argentina.

[e] Laboratorio Químico de Materiales Magnéticos Aplicados a la Ingeniería (LaQuiMMAI). Facultad de Ingeniería – UBA. Instituto de Química Aplicada a la Ingeniería (IQAI-UBA). Buenos Aires, Argentina.

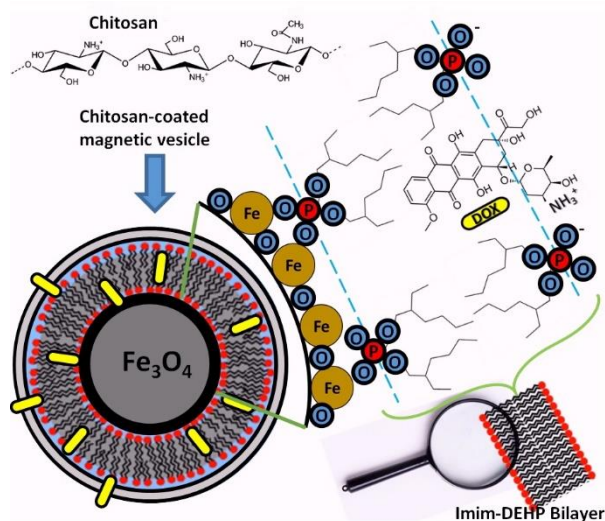
[f] Instituto de Investigaciones en Físico-Química de Córdoba (INFIQC-CONICET)- Departamento de Química Orgánica, Facultad de Ciencias Químicas, Universidad Nacional de Córdoba, Ciudad Universitaria, Córdoba, Argentina.

* Corresponding Authors: Dr. H. Andrada. handrada@exa.unrc.edu.ar;
Dr. Paula G. Bercoff. paula.bercoff@unc.edu.ar

Abstract

In this work, magnetic vesicles were produced using magnetite (Fe_3O_4) nanoparticles and 1-methylimidazolium bis-(2-ethylhexyl) phosphate (imim-DEHP) as surfactant. Some of the vesicles were subsequently coated with chitosan to improve their stability and biocompatibility. A physicochemical characterization of the prepared systems was carried out using several techniques, which allowed verifying that the magnetic nanoparticles were successfully encapsulated. Finally, the vesicles were loaded with an antitumor drug (doxorubicin) by swelling in order to perform release studies. The Korsmeyer-Peppas model was used to fit the doxorubicin (Dox) release profiles in the different vesicle systems, which displayed delayed release in every case. After 24 h, the Dox release percentages ranged between 43-53%. The prepared vesicles show not only excellent stability but also a good response to an external magnetic field, which makes them good candidates to be used in field-assisted therapies, thus trying to improve therapeutic efficacy and avoiding possible adverse effects.

TOC



Keywords: Imim-DEHP, vesicles, magnetite nanoparticles, chitosan, doxorubicin.

1. Introduction

Nanomedicine is a relatively new but rapidly developing area of knowledge in which materials in the nano-scale are used to deliver site-specific therapeutic agents in a controlled manner [1,2].

In recent years, important advances have been reported in this field for the treatment of various diseases, among them the use of chemotherapeutic agents, biological agents, immunotherapeutic agents, etc. [1–3]. Some of the drug nanocarriers that are currently under study for targeted therapies are based on magnetic nanoparticles (MNPs) [4–8]. Due to their size, as-prepared MNPs tend to aggregate forming micron-size clusters which do not exhibit the same magnetic behavior as individual MNPs. Furthermore, it has been reported that bare MNPs can cause obstructions in veins or arteries (embolisms) when they enter the bloodstream with no further treatment [9].

In order to overcome these drawbacks, MNPs are generally either coated with a layer of surfactant and/or biocompatible polymer or they are encapsulated in vesicles to improve their biocompatibility, to prevent oxidation and aggregate formation, as well as to avoid abduction by macrophages or phagocytic systems [5,9–16]. Chitosan (Ch) currently plays an extremely important role as a biomaterial, due to its diverse properties, such as good biocompatibility, biodegradability, bioactivity, anti thrombogenicity, low toxicity and low cost. Such properties are strongly dependent on the degree of deacetylation and its pK_a is around 6.5 [17,18]. Ch solubility depends on the distribution of free amino and N-acetyl groups, it is a linear polyelectrolyte at acidic pH, it dissolves slowly in acidic and slightly-acidic aqueous solutions besides being a hydrophilic molecule, it retains water in its structure and has the ability to form gels [19,20].

Vesicles have a spherical supramolecular structure formed by a bilayer of self-assembled surfactants (generally phospholipids) in aqueous solution [21]. They play an important role in encapsulating MNPs and provide the possibility of loading hydrophilic and hydrophobic bioactive molecules [4,9,14,22–26]. In particular, encapsulation of anthracyclines in vesicles, specifically doxorubicin (DOX), has the potential to decrease the toxicity of the agents. DOX is an antimicrobial and cytotoxic agent that intercalates in DNA and disrupts topoisomerase-II mediated DNA repair [27,28].

Various pharmaceutical formulations based on vesicular systems have been approved and many others are in the clinical trial stage [9,29–36]. Magnetic vesicles can be suitable for safe intravenous administration as nanocarriers in targeted therapies, when their sizes are below 200 nm [37,38].

At present, there are no reports of magnetic vesicles prepared from ionic liquids and biocompatible polymers. On the other hand, the formulations developed so far for the synthesis use several steps and the solution stability over time is low.

In this work, easily and rapidly prepared magnetic vesicles with high stability were synthesized using bis-(2-ethylhexyl) 1-methylimidazolium phosphate (imim-DEHP), an ionic liquid with amphiphilic properties that is able to spontaneously form unilamellar vesicles in water [21,39–41]. **Figure 1** shows a schematic of imim-DEHP. This novel surfactant -prepared in our group- facilitates the vesicles coating with chitosan. Magnetite (Fe_3O_4) nanoparticles were incorporated within the vesicles and this nanocomposite was coated with chitosan, to improve stability and biocompatibility. DOX was added to the vesicle structure as a test drug, and the behavior of the system was analyzed in order to assess its applicability for future use in field-assisted therapies [4,5,7,22,42–45].

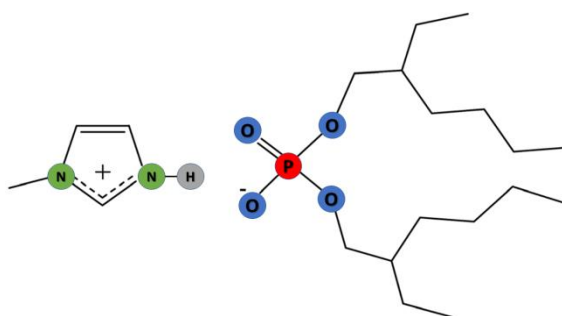


Figure 1. Scheme of the molecular structure of the surfactant imim-DEHP.

A complete structural characterization of the systems was carried out using X-ray Diffraction, Dynamic Light Scattering, Zeta potential, Atomic Force Microscopy, Scanning Electron Microscopy and Transmission Electron Microscopy.

The different compounds studied in this work were labeled as follows:

Ch: chitosan.

Mag: magnetite nanoparticles.

DOX: Doxorubicin.

Im: imim-DEHP vesicles.

Ch-Im: Chitosan-coated imim-DEHP vesicles.

Im-Mag: imim-DEHP vesicles loaded with magnetite nanoparticles without chitosan coating.

Ch-Im-Mag: Chitosan-coated imim-DEHP vesicles loaded with magnetite nanoparticles.

Ch-Im-Mag-DOX: Chitosan-coated imim-DEHP vesicles loaded with magnetite nanoparticles and DOX.

2. Experimental

2.1. Preparation of vesicles (*Im*)

Vesicles were prepared in aqueous medium from 1-methylimidazolium bis-(2-ethylhexyl) phosphate (**imim-DEHP**, $M_w=404.53$ g/mol) according to a previous work [21,39,40]. Chitosan (**Ch**) of low molecular weight (212.7 kDa or kg/mol) with a deacetylation degree of 79% was provided by *Sigma-Aldrich* and ultrapure water was obtained from *Labonco* equipment model 90901-01.

2.2. Preparation of magnetic nanoparticles (*MNPs*)

Magnetite NPs (Fe_3O_4 , $M_w \approx 231.53$ g/mol) were synthesized by coprecipitation, mixing an aqueous solution of $FeCl_2 \cdot 4H_2O$ (1.0 M) and $FeCl_3 \cdot 6H_2O$ (1.5 M) which had been previously flushed with N_2 . Once the reaction temperature was reached, an oxygen-free solution of NaOH 3 M was added (dropwise, slowly). The resulting solution was stirred for 2 h at 80°C. The obtained product was filtered and thoroughly washed with distilled water, ethanol and acetone several times. Each washing procedure was carried out until the filtrate became clear and colourless. The sample was finally dried at 40°C in a vacuum oven for 24 h.

2.3. Preparation of magnetic vesicles (*Im-Mag*)

To prepare the magnetic vesicles (approximately 5 wt. %) MNPs were first suspended in ultra-pure water by sonication. Immediately, a selected amount of imim-DEHP was added while the solution was vigorously stirred for approximately 2 min. Subsequently, a 0.45 μm nylon filter was used to remove undissolved solute or large aggregates.

2.4. Preparation of chitosan-coated magnetic vesicles (*Ch-Im-Mag*)

A 5×10^{-6} M **Ch** solution was prepared by dissolving 1 mg/ml in ultrapure water at pH=4 (with HCl) to dissolve the biopolymer; then it was neutralized with NaOH. Afterwards, 50 μl of this solution were added to the **Im-Mag** vesicle solution to obtain the biopolymer-coated vesicles. The resulting solution was manually stirred for approximately 1 min. Finally, the physicochemical characterization was performed.

2.5. Dynamic Light Scattering (DLS) and Zeta potential (ζ)

DLS measurements were carried out using a *Malvern 4700* equipment with a goniometer operating with *OBIS* 488 nm solid-state laser source (*Coherent Inc.*). To filter the solutions, a 0.45 μm pore size Nylon membrane filter (*Sartorius Brand*) was used. The samples were filtered in a quartz cell that was previously cleaned and rinsed with water. The scattered light was obtained at a 90° angle. The obtained data were assessed using the

CONTIN algorithm which is incorporated in the measuring instrument. The technique allows obtaining a size distribution and the apparent hydrodynamic diameter (D_H) can be calculated from the Stokes-Einstein equation:

$$D_H = kT/3\pi\eta D$$

where k is the Boltzmann constant, T is the absolute temperature, η is the solvent viscosity, and D is the translational diffusion coefficient [46,47]. Thirty independent size measurements for each surfactant concentration were performed with experimental errors of less than 5%.

The zeta potential of the vesicles was measured using DLS (*ZetasizerNano ZS Malvern Instrument Ltd.*) operating at 633 nm.

2.6. Morphological and Magnetic characterizations

Atomic Force Microscopy (AFM) measurements were performed in an *Agilent Technologies* Scanning Probe Microscope model 5500 working in acoustic AC mode, using probes with an aluminum reflective coating on the cantilever, with a force constant and a resonance frequency of ca. 5 N/m and 150 kHz respectively, and a tip radius below 10 nm (*Tap150Al-G; BudgetSensors®*). Freshly cleaved mica (muscovite grade V1; *Structure Probe, Inc.*) was used as a substrate. The vesicles were immobilized by electrostatic interaction on the bare mica surface. A few drops of the dispersion were deposited on the mica surface for 3-5 min before eliminating the excess by tilting the mica on a paper wipe. Finally, the mica was transferred to a desiccator containing silica gel (at room temperature and atmospheric pressure) until the surface was dry. The freshly prepared samples were mounted on the microscope and measured in air.

Scanning electron microscopy was conducted in a *Sigma Zeiss* Field Emission Scanning Electron microscope (FE-SEM) to characterize the magnetic NPs.

Transmission electron microscopy (TEM) images of the magnetic vesicles were obtained in a *JEOL* (JEM-EXXII 1200) microscope with a voltage of 80 kV.

The magnetic NPs hysteresis loop (magnetization M as a function of magnetic field H) was measured at room temperature in vibrating sample magnetometer Lakeshore 7300, applying magnetic fields between -1.5 and +1.5 T. For the measurement, the NPs were compacted in pellets.

2.7. Studies with doxorubicin (DOX)

A solution of 1×10^{-5} M **DOX** (Doxorubicin hydrochloride from *Sigma-Aldrich*, $M_w \approx 580$ g/Mol) was initially prepared in ultrapure water (Solution 1) to perform UV-visible and fluorescence tests. Then, Solution 2 was prepared by mixing Solution 1 with **Im** (1×10^{-2} M in water).

DOX release tests were carried out in ultrapure water at pH=7 and 25°C using *Franz* cells, using a high **DOX** concentration, 4.5×10^{-3} M (Solution 3). For these measurements, 1 ml of Solution 2 and Solution 3 (50:50) was prepared.

To favor **DOX** loading into the vesicle systems, the mixtures for sowing in the Franz cell were allowed to stand for 72 hours prior to the release measurements. The release was monitored by UV-visible measurements for 24 h, taking 1 ml samples from the acceptor compartment, and immediately refilling the removed volume with ultrapure water.

All experiments were carried out in duplicate.

3. Results and discussion

3.1. NPs characterization

XRD

The X-ray diffraction pattern of as-synthesized magnetite NPs is shown in **Figure 2**. The peaks observed at 18.3°, 30.1°, 35.5°, 37.1°, 43.1°, 53.5°, and 57.0° correspond to the crystal planes of the spinel phase: (111), (220), (311), (222), (400), (422), and (511), respectively (indexed with PDF file 00-001-1111) [48]. The well-

resolved peaks indicate the successful synthesis of magnetite NPs with a cubic inverse spinel structure. The presence of maghemite ($\gamma\text{-Fe}_2\text{O}_3$) in the final product cannot be disregarded, due to the very similar crystalline structure of these phases; however, this fact does not affect the overall magnetic properties of the NPs. The Scherrer size, calculated from the most intense peak at 37.1° yields $D_{Sch}=20$ nm. No secondary phases (other than the spinel structure) are noticed, within the detection limit of this technique.

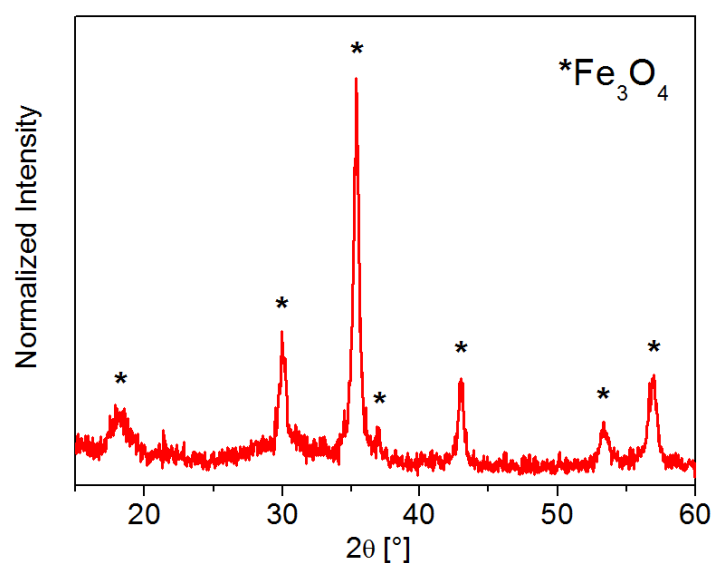


Figure 2. X-ray diffractogram of the as-produced magnetite NPs. The obtained phase corresponds to the spinel cubic structure.

TEM

As-synthesized magnetite NPs agglomerate in clusters as the one shown in **Figure S1**. The NPs mean size is 70 nm and they display a rather wide size distribution, as shown in the TEM image and the corresponding histogram of **Figure 3**. Considering that the crystallite size is $D_{Sch}=20$ nm, it is possible to conclude that the MNPs are polycrystalline.

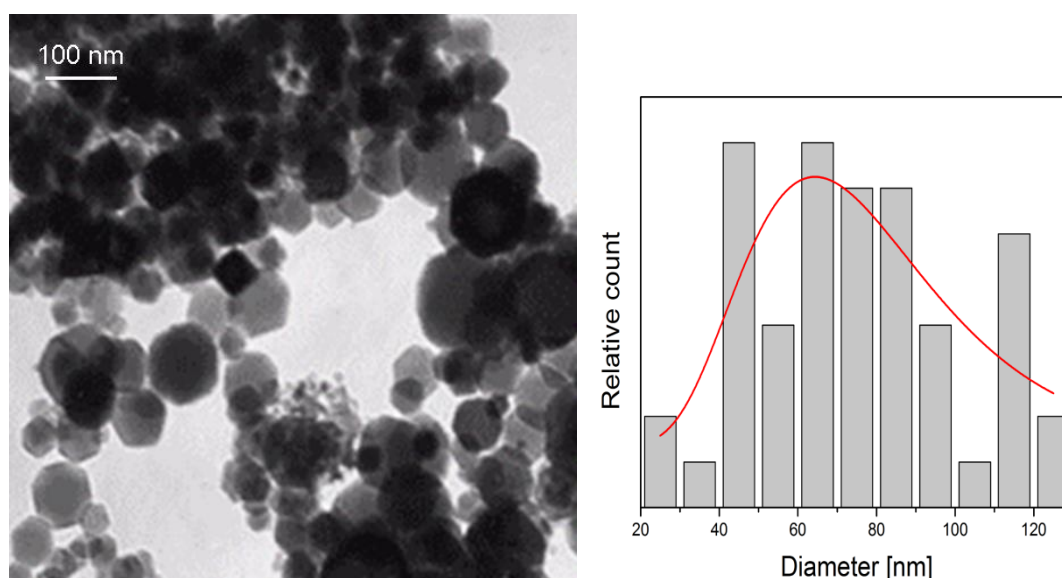


Figure 3. TEM image of as-produced magnetite NPs and size histogram.

Magnetic measurements

Figure 4 shows the hysteresis loop of synthesized magnetite NPs, which display a soft ferrimagnetic behavior, with coercivity values (H_c) of 11 mT and saturation magnetization (M_s) of 62 emu/g, in agreement with reported values for similar NPs of this phase [49].

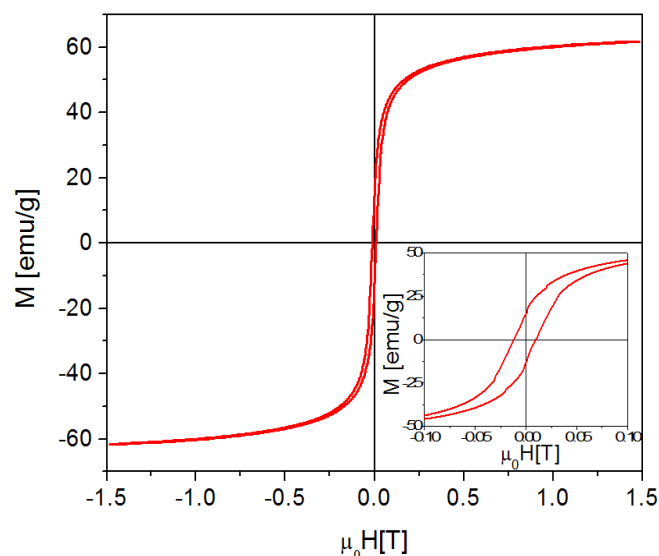


Figure 4. Hysteresis loop of magnetite NPs. The inset displays a close-up of the low-field region, where the small values of coercivity and remanence can be noticed.

It is noteworthy that the obtained NPs display a $\sim 70\%$ M_s value corresponding to micro-sized magnetite (~ 90 emu/g) [50]. As a consequence of being ferrimagnetic with a high M_s value despite the nanometric particles size -as opposed to smaller NPs which present superparamagnetic (SP) characteristics- these NPs are adequate to be easily manipulated by an external field in targeted therapies. In nanoparticulate systems, a commitment between size and performance must be achieved. On the other hand, larger MNPs are more suitable for a faster magnetic response, after appropriate coating in order to prevent flocculation.

Figure 4 shows that M_s is attained at relatively low fields, indicating a fast response to an external magnetic field, allowing an easy magnetic manipulation.

3.2. Vesicles characterization

Dynamic Light Scattering (DLS)

Figure 5a shows that **Im** size distributions present a hydrodynamic diameter of about 134 nm in ultra-pure water. This size increases to 152 nm when the NPs are included. In chitosan-coated vesicles (**Figure 5b**) the size increases to 180 nm and to 195 nm for **Ch-Im** and **Ch-Im-Mag**, respectively.

After chitosan addition, the same number of counts in DLS is obtained (by comparing the distributions shown in **Fig. 5a** and **5b**), this means that the vesicles had been covered and no new chitosan particles were generated in the solution. A small increase in the polydispersity index of the magnetic vesicles was also observed.

Table 1 shows that the vesicles' hydrodynamic diameter D_H increases with NPs inclusion and with chitosan coating in all cases, confirming the subsequent MNPs coating. Even when **Ch-Im-Mag** presents a $D_H = 195$ nm, this size is adequate for the application proposed in our work [9].

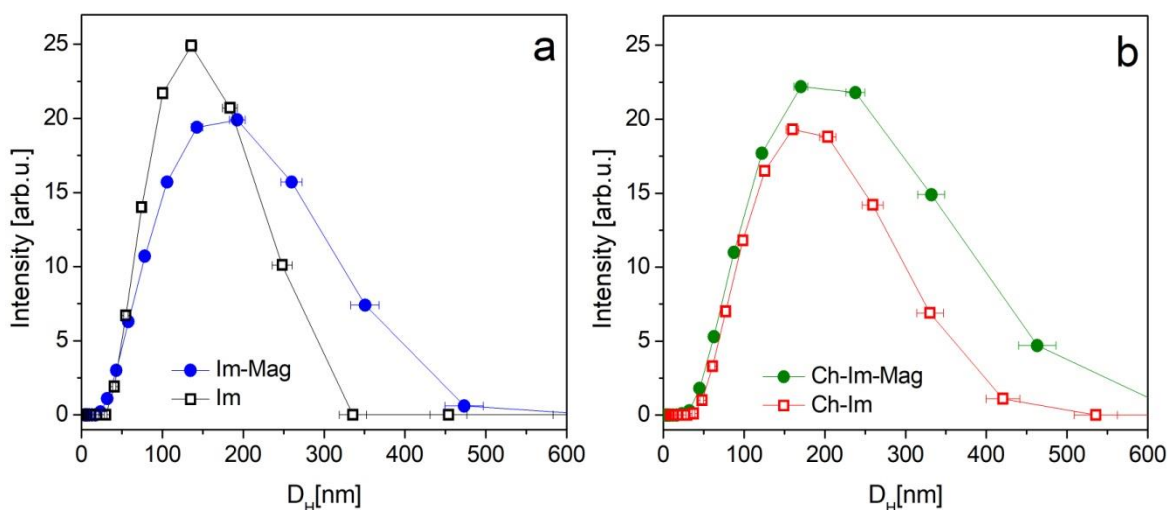


Figure 5. Vesicles size distributions before (a) and after (b) chitosan coating, as determined from DLS measurements performed in water, at pH = 7 and T = 25 °C.

Table 1. Hydrodynamic diameter D_H , polydispersity index PDI and Zeta potential values for the vesicles, both measurements conducted in ultrapure water at pH = 7 and T = 25 °C.

Vesicles	D_H [nm]	PDI	Zeta potential (ζ) [mV]
Im	134 ± 5	0.2	-33±2
Im-Mag	152 ± 7	0.3	-67±3
Ch-Im	180 ± 7	0.2	-29±2
Ch-Im-Mag	195 ± 9	0.3	-63±3
Ch-Im-Mag-DOX	-	-	-49±2

Zeta potential (ζ)

The zeta potential of the vesicles was measured using DLS (*ZetasizerNano ZS Malvern Instrument Ltd.*) operating at 633 nm.

From the data shown in **Table 1**, it can be seen that the **Im** zeta potential is negative (-33 mV) and it becomes even more negative (-67 mV) when encapsulating the MNPs. After chitosan addition, the zeta potential of **Ch-Im-Mag** increases towards more positive values, due to the positive charge of the polymer at pH=7. After **DOX** addition, a further increase of the zeta potential is observed (-49 mV), due to the effect of its positive charge on the vesicles' surface at pH=7 [51]. At this working pH the amine group belonging to chitosan is deprotonated because its $pK_a \approx 6$, so the polymer shows a nearly neutral charge, and for that reason no significant changes in the zeta potential are noticed [52,53].

Morphological characterization (AFM/TEM)

Figure 6 shows AFM images of **Ch-Im** (a) and **Ch-Im-Mag** (b). The vesicles present spherical symmetry, with an approximate height of ca. 50 nm and a diameter of ca. 250 nm. The observed slight deformation and the different size compared to results obtained by DLS are due to the crushing of the vesicles against the mica surface, probably due to the electrostatic interactions that the sample undergoes after being deposited [54–56].

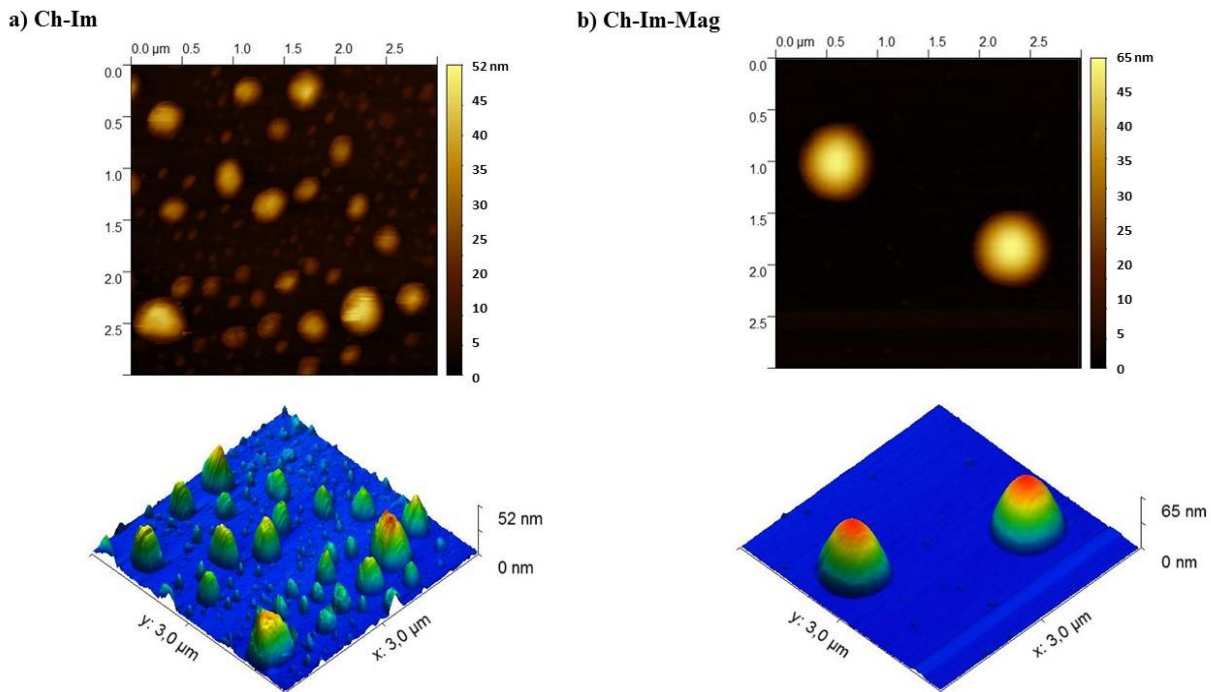


Figure 6. AFM images (top view and 3-D maps) of the scanned $3\ \mu\text{m} \times 3\ \mu\text{m}$ areas corresponding to samples a) **Ch-Im** and b) **Ch-Im-Mag**.

Figure 7 shows a TEM image of **Ch-Im-Mag**, which confirms that these vesicles have spherical symmetry and that their size is in agreement with results from DLS and AFM. The MNPs within the vesicles can be noticed as a darker contrast in the image. An empty vesicle can also be noticed in the figure.

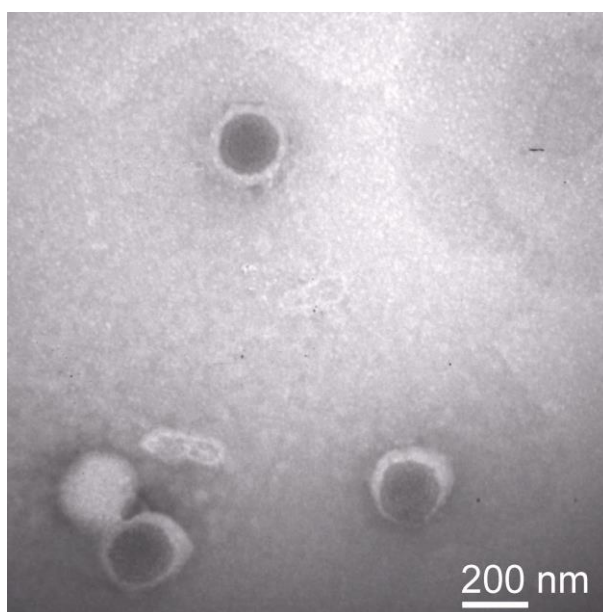


Figure 7. TEM image of **Ch-Im-Mag** in which the MNPs can be seen within the vesicles. This image also shows the presence of an empty vesicle.

Suspension stability

Figure 8 (left) shows that the magnetic vesicles are well dispersed in water. When applying a magnetic field, the vesicles agglomerate due to the magnetic force (central image). A detail of this image is presented on **Figure 8** (right). After removing the magnetic field and manually shaking the solution, the vesicles are easily resuspended showing an excellent stability as no precipitates are observed.

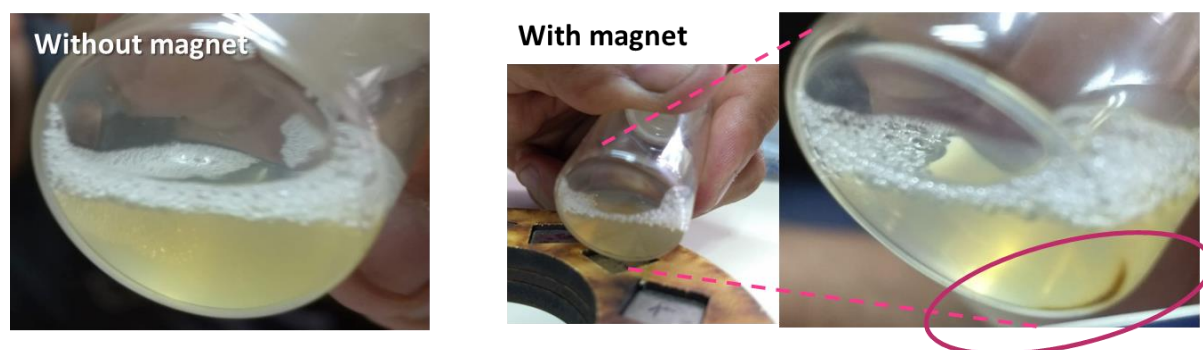


Figure 8. Ch-Im-Mag solution, without and with an applied magnetic field.

In order to test the suspension stability over time, DLS measurements were repeated after one year of preparation. A value of $D_H = (223 \pm 9)$ nm and a PDI of 0.3 were obtained, confirming **Ch-Im-Mag** great stability over time, since D_H only increased by about 10% and its PDI remained constant.

3.3. DOX Interaction studies and release experiments

The interaction between **DOX** and the bare vesicles (**Im**) was characterized by absorption and emission spectroscopies. In particular, Red Edge Excitation Shift (REES) effect was used as a tool to determine if **DOX** molecules are located inside the vesicles' bilayer [57].

The observation of REES is related to the **DOX** environment. The Franck-Condon principle implies that a fluorophore interacting (via dipole-dipole mechanism) with the solvent molecules of the environment will have a reduced energy separation between the fundamental and first excited states (solvent relaxation), resulting in a red shift of the fluorescence emission [58]. When the solvent polarity increases, a further reduction in the energy level of the excited state of the fluorophore correspondingly occurs. Also, the polarity of the fluorophore determines how sensitive the first excited state is to changes in the solvent. Therefore, a stronger effect (red shift) is observed in polar and/or charged fluorophores as compared to non-polar fluorophores [59].

UV-Visible spectra of **DOX** in ultra-pure water as a function of **Im** concentration are shown in **Figure S2**. A shift of the band located at 495 nm towards higher wavelengths was observed with increasing vesicle concentration, which indicates that **DOX** diffuses towards an environment of lower polarity, suggesting that **DOX** is located in the vesicles bilayer [60].

Figure 9 shows emission fluorescence spectra in different conditions: (a) **DOX** (1×10^{-5} M) in water and in **Im-DOX** ($[\text{Im}] = 1 \times 10^{-2}$ M) using different excitation wavelengths, $\lambda_{\text{ex}} = 450, 500$ and 550 nm; and (b) Varying **Im** concentration with fixed λ_{ex} (550 nm, $[\text{DOX}] 1 \times 10^{-5}$ M). The REES values were calculated using the following expression:

$$REES = \Delta\lambda_{em} = (\lambda_{em(\lambda_{ex}550nm)} - \lambda_{em(\lambda_{ex}450nm)})$$

where λ_{em} corresponds to the wavelength of the emission maximum of each excitation wavelength λ_{ex} .

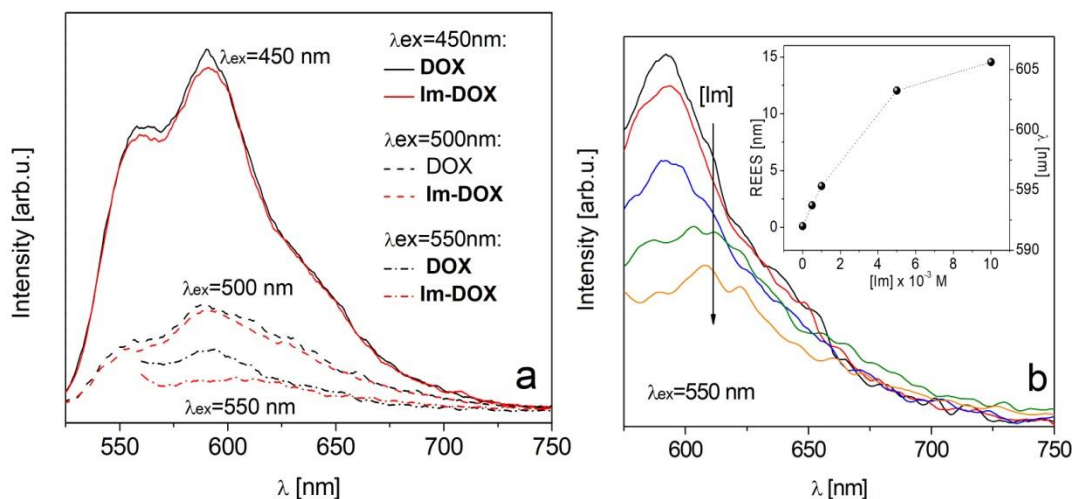


Figure 9. (a) Fluorescence spectra of **DOX** and **Im-DOX** dispersed in ultra pure water at pH=7, for different excitation wavelengths (λ_{ex} =450, 500 and 550 nm). $[\text{DOX}] = 1 \times 10^{-5}$ M. (b) **DOX** fluorescence spectra at different **Im** concentrations (dispersed in ultra-pure water at pH=7) for an excitation wavelength of 550 nm. $[\text{DOX}] = 1 \times 10^{-5}$ M. The vertical arrow indicates an increase in **Im** concentration from 0 M to 1×10^{-2} M. The inset shows REES values at the **DOX** maximum emission wavelength as a function of **Im** concentration. $[\text{DOX}] = 1 \times 10^{-5}$ M.

A wavelength shift in the maximum emission is not observed before the addition of **Im** for excitation wavelengths of 450 and 500 nm, as shown in **Figures S3** and **S4** where fluorescence as a function of **Im** concentration is displayed. The decrease of fluorescence intensity observed for all λ_{ex} may be a consequence of **DOX** interaction with **Im** phosphate groups [61–64], located in the vesicle bilayer.

The inset in **Figure 9b** shows that REES values increase as a function of **Im** concentration. A REES value = 0 in absence of vesicles is consistent with the drug being completely soluble in water. However, when the imimDEHP concentration increases (and the vesicles are formed) the REES value increases, indicating the incorporation of **DOX** in a more viscous region (the bilayer). After vesicle formation ($[\text{ImimDEHP}]$ greater than the critical vesicular concentration) [21] a REES value greater than 10 is obtained. This unusual value cannot be explained by only taking into account the environment's viscosity [65] but it can be rationalized considering that two processes take place: **DOX** electrostatic surface interaction with **Im** phosphate groups [57,65–69], and **DOX** diffusion through the vesicles' bilayer as a consequence of the bilayer's less polar medium.

Kwok et al. propose an interaction between the O⁻/OH belonging to **DOX** and the NPs superficial Fe ions through the formation of a Fe-OH complex [70]. Bhatta et al studied the interaction between **DOX** and **Ch**, showing that it is mediated by the H bonds between the OH groups from **Ch** and the NH₂ groups from the **DOX** and/or by retention at the **Ch** polymeric network [71]. We propose a multiple interaction between the **DOX** molecule and the magnetic vesicles, through which the drug can be attached: 1) Some **DOX** interacts with the superficial **Ch** coating through H bonds; 2) some **DOX** is located within the imim-DEHP bilayer, subject to an electrostatic interaction between PO₄³⁻ and NH₃⁺ groups (see **Figure 10a**). As the **DOX** molecule is located within the bilayer, a hydrophobic interaction is also present (the surfactant non-polar chains can host the **DOX** non-polar groups within the bilayer); and 3) a small **DOX** amount might interact with the superficial Fe atoms of the MNPs (**Figure 10b**).

Figure 10a displays a scheme of the possible **DOX** location within the **Im** bilayer.

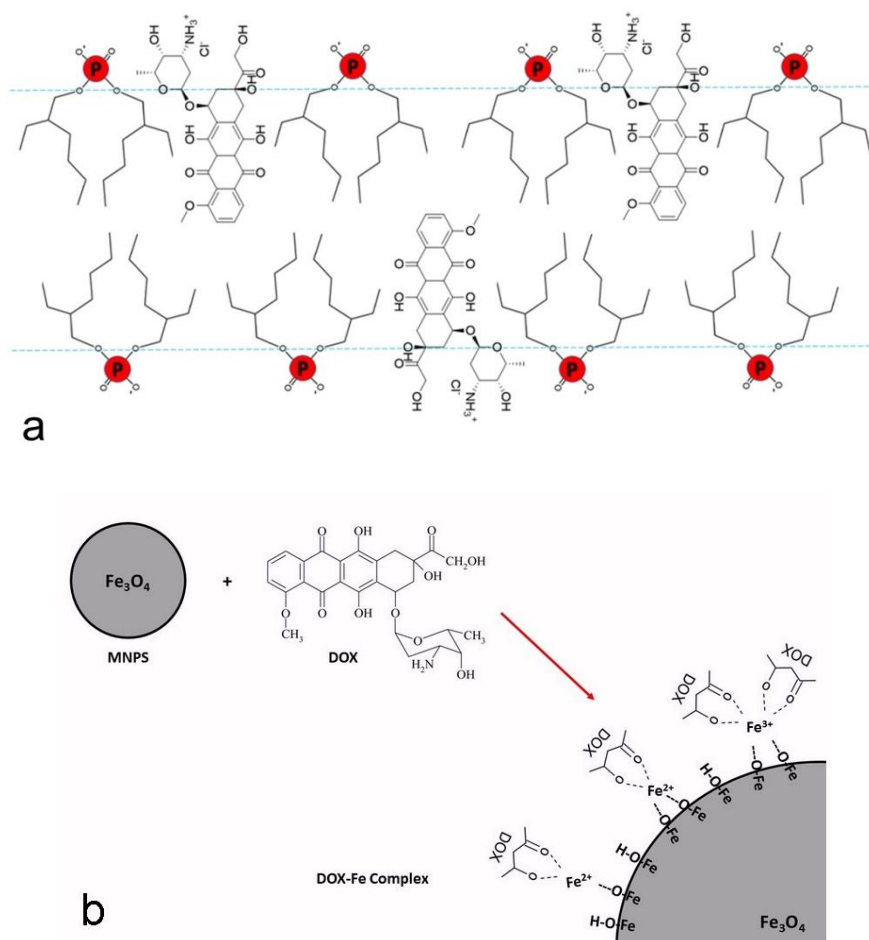


Figure 10. (a) Schematic representation of DOX's possible location in the vesicles' bilayer. The top corresponds to the outer part of the spherical vesicle. (b) Interaction between DOX and MNPs superficial Fe. (Own designs).

Im, **Im-Mag** and **Ch-Im-Mag** were selected to perform **DOX** release experiments. The vesicles were loaded with **DOX** and in order to calculate the **DOX** encapsulation efficiency in the different vesicle systems, 1 ml of the seeding solutions was filtered through a polycarbonate filter of 0.1 μm pore size. The solutions obtained from the filtrate were analyzed by UV-visible. The encapsulation efficiency (EE) of **DOX** was calculated using the equation:

$$EE(\%) = \frac{[Total\ DOX] - [Free\ DOX]}{[Total\ DOX]} \times 100$$

obtaining an EE higher than 97% in all cases.

Then, release studies using Franz cells were carried out, in order to evaluate their functionality [72].

Figure 11a shows the kinetic release profile for all the studied samples. After 1 h, all the vesicles release a similar amount of **DOX** (between 4-5%, see **Table 2**) probably due to the spontaneous release of the **DOX** that remained attached to the vesicles surface [73,74].

During the first 7 h **Ch-Im-Mag** presents a relative delay compared to **Im-Mag** and **Im**, as the **DOX** molecules inside the vesicles need to go through both chitosan and the bilayer during release. An increase in the release rate of this sample is observed at times close to 24 h (see **Figure 11a**), which could be accounted for by chitosan swelling and/or erosion [28,73,74], this latter understood by the loss of polymer from the vesicles surface. Studies of chitosan-based structures have shown that after 24h and in buffer solutions at or below pH=6.5, these structures exhibit a 44 % increased erosion as compared to neutral ones [75]. While the exact mechanism was not described, it was postulated that the erosion increment is due to the protonation of chitosan's surface layers [76]. In our study, the loss of chitosan bound to the vesicles surface can be explained

considering the release of protonated **DOX** (**DOXH⁺**, **Figure 10a**). This process generates a protogenic effect due to the exchange process **H⁺/DOXH⁺** [77,78], thus an increased proportion of chitosan acquires positive charge. Further experiments are needed to conclude about this mechanism.

In the case that **DOX** molecules reach the MNPs surface through the bilayer, **DOX-Fe** interaction could also contribute to **DOX** retention. This can be explained through iron chelation with the carbonyl and hydroxyl **DOX** groups (**Figure 11**). **DOX-Fe** complexes have been previously reported by other authors in similar systems [78–81].

The maximum amount of released **DOX** at 24 h is related to the vesicle's nature. **Im** and **Im-Mag** reach similar values (ca. 44%). Sample **Ch-Im-Mag** releases the highest **DOX** amount after 24 h (53%). The kinetic release profile corresponding to **Im-Mag** displays a delay in the release process after 7 h (compared to **Im**), attributed to the interaction between the MNPs and the double layer. This effect can be explained by the O-P interactions between the external MNPs oxygen atoms and the phosphate groups of the bilayer, as indicated in the schemes of **Figure 10**. This effect may reduce the bilayer's fluidity, which in turn increases **DOX** retention, within the bilayer.

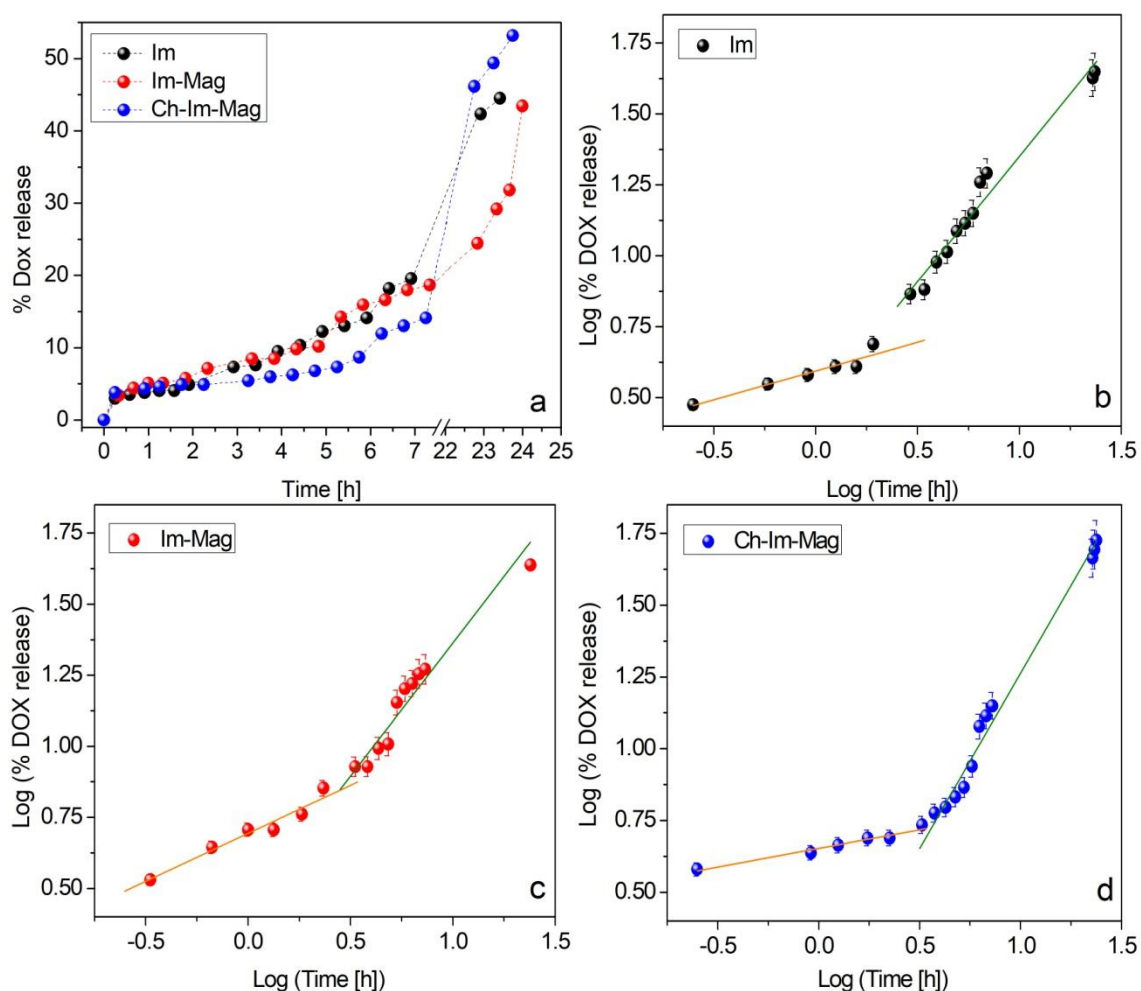


Figure 11. (a) **DOX** release as a function of time for the different vesicles. Log-Log plots of **DOX** release for **Im** (b), **Im-Mag** (c) and **Ch-Im-Mag** (d). The solid lines correspond to the fits using Korsmeyer-Peppas model from 0.2 to 2 h (*stage I*: orange line) and from 2 to 24 h (*stage II*: green line).

In order to describe the release processes, the Korsmeyer-Peppas model was used [82]:

$$C_t/C_0 = kt^n$$

where C_t/C_0 is the released fraction at time t , k is a constant and n is the release exponent which characterizes the release mechanism.

As shown in **Figures 11b, 11c** and **11d**, linear fits in log-log plots allow identifying two stages for each sample (*stage I* from 0.2 to 2 h, and *stage II* from 2 to 24 h), each of which is associated with a different behavior. The fitting parameters and correlation coefficients are presented in **Table 2** together with the fitting regression coefficients (R^2), which were all over 0.92 indicating a good correlation. In equation (1), the parameter n can take a range of values that indicate the type of transport. When $0 < n < 0.5$, the active compound is released by simple Fickian diffusion, while when $0.5 < n < 1.0$, the diffusion process is a combination of Fickian and non-Fickian diffusion, and it is known as ‘anomalous diffusion’.

Table 2. Fitting parameters k (constant) and n (release exponent) calculated with Korsmeyer-Peppas model for the studied samples. The regression coefficient R^2 is also listed.

Sample	Stage	k [h ⁻ⁿ]	n	R^2
Im	I	3.9 ± 0.1	0.20 ± 0.03	0.9245
	II	2.9 ± 0.3	0.88 ± 0.06	0.9606
Im-Mag	I	4.9 ± 0.1	0.34 ± 0.03	0.9535
	II	2.7 ± 0.4	0.94 ± 0.09	0.9242
Ch-Im-Mag	I	4.5 ± 0.1	0.13 ± 0.01	0.9631
	II	1.1 ± 0.1	1.22 ± 0.06	0.9723

Considering the Korsmeyer-Peppas model, the fact that in *stage I* the release exponents (n) remain below 0.5 for every sample, suggests that a *Fickian* mechanism (diffusion process) for spherical vesicles is occurring [82]. In *stage II*, as $0.5 < n < 1.0$, an *anomalous* (non *Fickian*) diffusion is observed for **Im** and **Im-Mag**, indicating that the release mechanism in these cases also involves swelling of the vesicles, as well as diffusion [82].

Only in sample **Ch-Im-Mag** it is $n > 1$, in *stage II*. In this case, an extreme type of diffusion mechanism is involved (known as Super Case II). This behavior can be related to the polymer relaxation which enhances water penetration [83] which may affect the **DOX** release mechanism. The different behaviors between **Im** and **Im-Mag** compared to **Ch-Im-Mag** in *stage II*, can be attributed to the fact that the velocity of water penetration in the first two vesicles is lower than in **Ch-Im-Mag** as they do not have **Ch** coating [85].

4. Conclusion

In this work, Imim-DEHP vesicles were obtained by a one-step preparation method. The chitosan-coated vesicles show great stability in solution, and no significant changes in size were detected over a year.

Magnetite NPs were successfully encapsulated into the vesicles and thoroughly characterized. Chitosan-coated magnetic vesicles (**Ch-Im-Mag**) suspended in water can be easily manipulated by an external magnetic field.

Furthermore, the vesicles were able to load and release a bioactive molecule, such as the antitumor drug doxorubicin. The inclusion of MNPs in the vesicles allows easy manipulation while keeping their loading capacity, yet somewhat reducing the drug’s release rate due to the interaction between the MNPs surface and the vesicle’s bilayer, through the phosphate groups.

The novel prepared system (chitosan-coated magnetic vesicles) is a good candidate for testing in field-assisted therapies due to its fast response to magnetic fields. It is important to remark that all experiments were

performed at pH=7 and room temperature. In future work, it is intended to continue with biocompatibility and cytotoxicity studies. Cytotoxicity tests will be carried out in cell cultures and possible alterations in basic cellular functions will be evaluated.

Acknowledgments

Financial support from the Consejo Nacional de Investigaciones Científicas y Técnicas (PIP CONICET 112-2015-0100283), Universidad Nacional de Río Cuarto (PPI-UNRC 2016-2019), Agencia Nacional de Promoción Científica y Técnica (PICT 2019-0543), Universidad Nacional de Córdoba (UNC) and Ministerio de Ciencia y Tecnología (Mincyt), is gratefully acknowledged. O.F.S., R.D.F. and P.G.B. hold research positions at CONICET. H. E. A. and L. V. thank CONICET for post-doctoral fellowships.

ELECTRONIC SUPPLEMENTARY INFORMATION

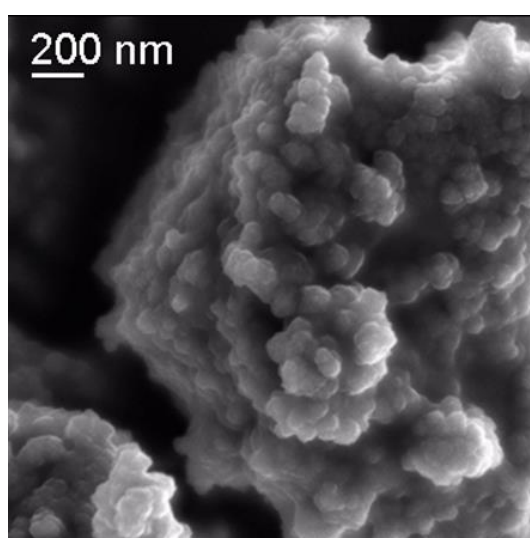


Figure S1. SEM image of as-produced magnetite NPs.

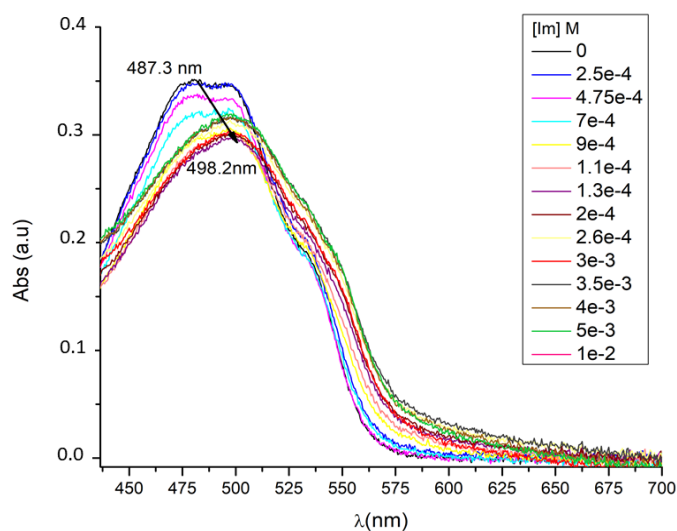


Figure S2. UV-visible spectrum of DOX as a function of Im concentration. [DOX]= 1×10^{-5} M.

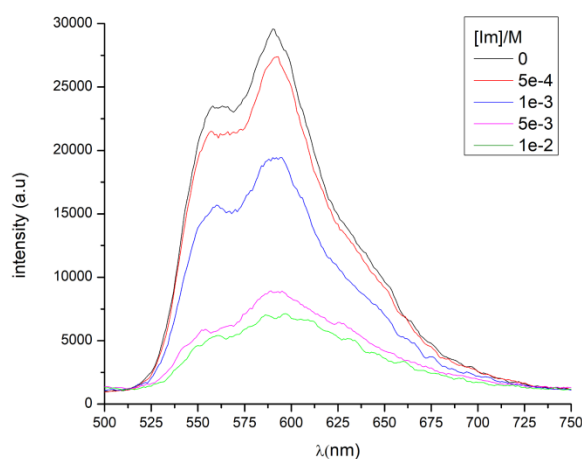


Figure S3. DOX Fluorescence Spectra as a function of Im concentration. Vesicles dispersed in ultra-pure water at pH = 7, for an excitation wavelength of 450 nm. [DOX]= 1×10^{-5} M.

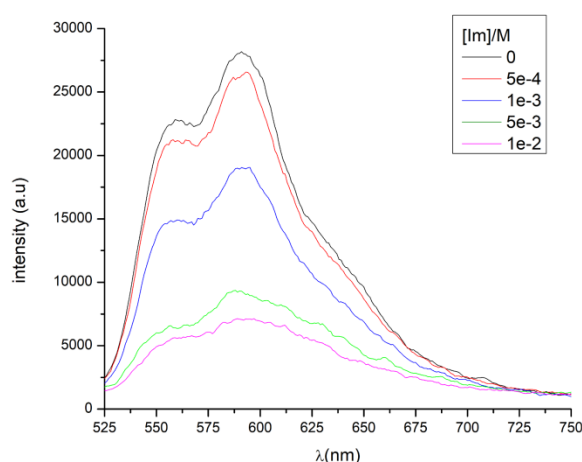


Figure S4. DOX Fluorescence Spectra as a function of Im concentration. Vesicles dispersed in ultra-pure water at pH = 7, for an excitation wavelength of 500 nm. [DOX]= 1×10^{-5} M.

References

- [1] H.M. Abdel-Mageed, N.Z. AbuelEzz, R.A. Radwan, S.A. Mohamed, Nanoparticles in nanomedicine: a comprehensive updated review on current status, challenges and emerging opportunities, *J. Microencapsul.* 38 (2021) 414–436. <https://doi.org/10.1080/02652048.2021.1942275>.
- [2] B. Dutta, K.C. Barick, P.A. Hassan, Recent advances in active targeting of nanomaterials for anticancer drug delivery, *Adv. Colloid Interface Sci.* 296 (2021) 102509. <https://doi.org/https://doi.org/10.1016/j.cis.2021.102509>.
- [3] A. Samide, B. Tutunaru, R.M. Varut, B. Oprea, S. Iordache, Interactions of some chemotherapeutic agents as epirubicin, gemcitabine and paclitaxel in multicomponent systems based on orange essential oil, *Pharmaceuticals.* 14 (2021). <https://doi.org/10.3390/ph14070619>.
- [4] J. Nogueira, S.F. Soares, C.O. Amorim, J.S. Amaral, C. Silva, F. Martel, T. Trindade, A.L. Daniel-Da-Silva, Magnetic driven nanocarriers for pH-responsive doxorubicin release in cancer therapy, *Molecules.* 25 (2020) 1–21. <https://doi.org/10.3390/molecules25020333>.
- [5] G. Ak, Ş. Hamarat Şanlıer, Erythrocyte membrane vesicles coated biomimetic and targeted doxorubicin nanocarrier: Development, characterization and in vitro studies, *J. Mol. Struct.* 1205 (2020). <https://doi.org/10.1016/j.molstruc.2019.127664>.
- [6] B. Mehrafrooz, M.Z. Pedram, E. Ghafar-Zadeh, An improved method for magnetic nanocarrier drug delivery across the cell

- membrane, *Sensors* (Switzerland). 18 (2018) 1–15. <https://doi.org/10.3390/s18020381>.
- [7] P.C. Liang, Y.C. Chen, C.F. Chiang, L.R. Mo, S.Y. Wei, W.Y. Hsieh, W.L. Lin, Doxorubicin-modified magnetic nanoparticles as a drug delivery system for magnetic resonance imaging-monitoring magnet-enhancing tumor chemotherapy, *Int. J. Nanomedicine*. 11 (2016) 2021–2037. <https://doi.org/10.2147/IJN.S94139>.
- [8] M. Zhalechin, S.M. Dehaghi, M. Najafi, A. Moghimi, Magnetic polymeric core-shell as a carrier for gradual release in-vitro test drug delivery, *Heliyon*. 7 (2021). <https://doi.org/10.1016/j.heliyon.2021.e06652>.
- [9] O. Bixner, E. Reimhult, Controlled magnetosomes: Embedding of magnetic nanoparticles into membranes of monodisperse lipid vesicles, *J. Colloid Interface Sci.* 466 (2016) 62–71. <https://doi.org/10.1016/j.jcis.2015.11.071>.
- [10] S. Lecommandoux, O. Sandre, F. Chécot, J. Rodriguez-Hernandez, R. Perzynski, Magnetic nanocomposite micelles and vesicles, *Adv. Mater.* 17 (2005) 712–718. <https://doi.org/10.1002/adma.200400599>.
- [11] A. Kulshrestha, P.S. Gehlot, A. Kumar, Magnetic proline-based ionic liquid surfactant as a nano-carrier for hydrophobic drug delivery, *J. Mater. Chem. B*. 8 (2020) 3050–3057. <https://doi.org/10.1039/d0tb00176g>.
- [12] F. Ye, Å. Barrefelt, H. Asem, M. Abedi-Valugerdi, I. El-Serafi, M. Saghafian, K. Abu-Salah, S. Alrokayan, M. Muhammed, M. Hassan, Biodegradable polymeric vesicles containing magnetic nanoparticles, quantum dots and anticancer drugs for drug delivery and imaging, *Biomaterials*. 35 (2014) 3885–3894. <https://doi.org/10.1016/j.biomaterials.2014.01.041>.
- [13] A. Mateos-Maroto, A. Guerrero-Martínez, R.G. Rubio, F. Ortega, F. Martínez-Pedrero, Magnetic Biohybrid Vesicles Transported by an Internal Propulsion Mechanism, *ACS Appl. Mater. Interfaces*. 10 (2018) 29367–29377. <https://doi.org/10.1021/acsami.8b09862>.
- [14] D. Fan, J. Hao, Magnetic aligned vesicles, *J. Colloid Interface Sci.* 342 (2010) 43–48. <https://doi.org/10.1016/j.jcis.2009.10.013>.
- [15] J.C. Bacri, V. Cabuil, A. Cebers, C. Ménager, R. Perzynski, Magnetic vesicles, *Mater. Sci. Eng. C*. 2 (1995) 197–203. [https://doi.org/10.1016/0928-4931\(95\)00076-3](https://doi.org/10.1016/0928-4931(95)00076-3).
- [16] J. Alonso, H. Khurshid, J. Devkota, Z. Nemat, N.K. Khadka, H. Srikanth, J. Pan, M.H. Phan, Superparamagnetic nanoparticles encapsulated in lipid vesicles for advanced magnetic hyperthermia and biodetection, *J. Appl. Phys.* 119 (2016) 1–7. <https://doi.org/10.1063/1.4942618>.
- [17] M. Ashrafizadeh, Z. Ahmadi, N. Mohamadi, A. Zarrabi, S. Abasi, G. Dehghannoudeh, R.N. Tamaddondoust, H. Khanbabaeei, R. Mohammadnejad, V.K. Thakur, Chitosan-based advanced materials for docetaxel and paclitaxel delivery: Recent advances and future directions in cancer theranostics, *Int. J. Biol. Macromol.* 145 (2020) 282–300. <https://doi.org/10.1016/J.IJBIOMAC.2019.12.145>.
- [18] G. Salmanian, S.A. Hassanzadeh-Tabrizi, N. Koupaei, Magnetic chitosan nanocomposites for simultaneous hyperthermia and drug delivery applications: A review, *Int. J. Biol. Macromol.* 184 (2021) 618–635. <https://doi.org/10.1016/j.ijbiomac.2021.06.108>.
- [19] M. Fathi, Á. Martín, D.J. McClements, Nanoencapsulation of food ingredients using carbohydrate based delivery systems, *Trends Food Sci. Technol.* 39 (2014) 18–39. <https://doi.org/10.1016/j.tifs.2014.06.007>.
- [20] A. Ali, S. Ahmed, A review on chitosan and its nanocomposites in drug delivery, *Int. J. Biol. Macromol.* 109 (2018) 273–286. <https://doi.org/10.1016/j.ijbiomac.2017.12.078>.
- [21] H.E. Andrada, O.F. Silva, G.M. Morales, N.M. Correa, R.D. Falcone, Spontaneous formation of unilamellar vesicles based on the surfactant 1-methylimidazolium bis-(2-ethylhexyl) phosphate, evaluated as a function of pH and in saline solution, *Colloids Surfaces A Physicochem. Eng. Asp.* 606 (2020) 125435. <https://doi.org/10.1016/j.colsurfa.2020.125435>.
- [22] C. Sanson, O. Diou, J. Thévenot, E. Ibarboure, A. Soum, A. Brûlet, S. Miraux, E. Thiaudière, S. Tan, A. Brisson, V. Dupuis, O. Sandre, S. Lecommandoux, Doxorubicin loaded magnetic polymersomes: Theranostic nanocarriers for MR imaging and magneto-chemotherapy, *ACS Nano*. 5 (2011) 1122–1140. <https://doi.org/10.1021/nn102762f>.
- [23] S. Nigam, D. Bahadur, Doxorubicin-loaded dendritic-Fe₃O₄ supramolecular nanoparticles for magnetic drug targeting and tumor regression in spheroid murine melanoma model, *Nanomedicine Nanotechnology, Biol. Med.* 14 (2018) 759–768. <https://doi.org/10.1016/j.nano.2018.01.005>.
- [24] V. Plassat, C. Wilhelm, V. Marsaud, C. Ménager, F. Gazeau, J.M. Renoir, S. Lesieur, Anti-estrogen-loaded superparamagnetic liposomes for intracellular magnetic targeting and treatment of breast cancer tumors, *Adv. Funct. Mater.* 21 (2011) 83–92. <https://doi.org/10.1002/adfm.201001450>.
- [25] K.Y. Vlasova, A. Piroyan, I.M. Le-Deygen, H.M. Vishwasrao, J.D. Ramsey, N.L. Klyachko, Y.I. Golovin, P.G. Rudakovskaya, I.I. Kireev, A. V. Kabanov, M. Sokolsky-Papkov, Magnetic liposome design for drug release systems responsive to super-low frequency alternating current magnetic field (AC MF), *J. Colloid Interface Sci.* 552 (2019) 689–700. <https://doi.org/10.1016/j.jcis.2019.05.071>.
- [26] P. Xing, Y. Zhao, Supramolecular Vesicles for Stimulus-Responsive Drug Delivery, *Small Methods*. 2 (2018) 1700364. <https://doi.org/10.1002/smt.201700364>.
- [27] C.F. Thorn, C. Oshiro, S. Marsh, T. Hernandez-Boussard, H. McLeod, T.E. Klein, R.B. Altman, Doxorubicin pathways: Pharmacodynamics and adverse effects, *Pharmacogenet. Genomics*. 21 (2011) 440–446. <https://doi.org/10.1097/FPC.0b013e32833ffb56>.
- [28] T. Wu, S. Yu, D. Lin, Z. Wu, J. Xu, J. Zhang, Z. Ding, Y. Miao, T. Liu, T. Chen, X. Cai, Preparation, Characterization, and Release Behavior of Doxorubicin hydrochloride from Dual Cross-Linked Chitosan/Alginate Hydrogel Beads, *ACS Appl. Bio Mater.* 3 (2020) 3057–3065. <https://doi.org/10.1021/acsabm.9b01119>.
- [29] J. Yu, Y. Wang, S. Zhou, J. Li, J. Wang, D. Chi, X. Wang, G. Lin, Z. He, Y. Wang, Remote loading paclitaxel–doxorubicin prodrug into liposomes for cancer combination therapy, *Acta Pharm. Sin. B*. (2020). <https://doi.org/10.1016/j.apsb.2020.04.011>.
- [30] N. Takahashi, K. Higashi, K. Ueda, K. Yamamoto, K. Moribe, Determination of Nonspherical Morphology of Doxorubicin-Loaded Liposomes by Atomic Force Microscopy, *J. Pharm. Sci.* 107 (2018) 717–726. <https://doi.org/10.1016/j.xphs.2017.10.009>.
- [31] G. Varan, C. Varan, N. Erdoğan, A.A. Hincal, E. Bilensoy, Amphiphilic cyclodextrin nanoparticles, *Int. J. Pharm.* 531 (2017)

- 457–469. <https://doi.org/10.1016/j.ijpharm.2017.06.010>.
- [32] O.F. Silva, R.H. De Rossi, N.M. Correa, J.J. Silber, R.D. Falcone, Spontaneous catanionic vesicles formed by the interaction between an anionic β -cyclodextrins derivative and a cationic surfactant, *RSC Adv.* 8 (2018) 12535–12539. <https://doi.org/10.1039/c8ra01482e>.
- [33] A. Abruzzo, B. Giordani, C. Parolin, B. Vitali, M. Protti, L. Mercolini, M. Cappelletti, S. Fedi, F. Bigucci, T. Cerchiara, B. Luppi, Novel mixed vesicles containing lactobacilli biosurfactant for vaginal delivery of an anti-Candida agent, *Eur. J. Pharm. Sci.* 112 (2018) 95–101. <https://doi.org/10.1016/j.ejps.2017.11.012>.
- [34] Y. Barenholz, Doxil® - The first FDA-approved nano-drug: Lessons learned, *J. Control. Release.* 160 (2012) 117–134. <https://doi.org/10.1016/j.jconrel.2012.03.020>.
- [35] M. Qiu, H. Sun, F. Meng, R. Cheng, J. Zhang, C. Deng, Z. Zhong, Lipopepsomes: A novel and robust family of nano-vesicles capable of highly efficient encapsulation and tumor-targeted delivery of doxorubicin hydrochloride in vivo, *J. Control. Release.* 272 (2018) 107–113. <https://doi.org/10.1016/j.jconrel.2018.01.011>.
- [36] K. Zabielska-Koczywaś, R. Lechowski, The use of liposomes and nanoparticles as drug delivery systems to improve cancer treatment in dogs and cats, *Molecules.* 22 (2017). <https://doi.org/10.3390/molecules22122167>.
- [37] S. Hejmady, R. Pradhan, A. Alexander, M. Agrawal, G. Singhvi, B. Gorain, S. Tiwari, P. Kesharwani, S.K. Dubey, Recent advances in targeted nanomedicine as promising antitumor therapeutics, *Drug Discov. Today.* 25 (2020) 2227–2244. <https://doi.org/10.1016/j.drudis.2020.09.031>.
- [38] H. Chugh, D. Sood, I. Chandra, V. Tomar, G. Dhawan, R. Chandra, Role of gold and silver nanoparticles in cancer nanomedicine, *Artif. Cells, Nanomedicine Biotechnol.* 46 (2018) 1210–1220. <https://doi.org/10.1080/21691401.2018.1449118>.
- [39] N. Dib, J.J. Silber, N.M. Correa, R.D. Falcone, Combination of a protic ionic liquid-like surfactant and biocompatible solvents to generate environmentally friendly anionic reverse micelles, *New J. Chem.* 43 (2019) 10398–10404. <https://doi.org/10.1039/C9NJ02268F>.
- [40] C.M.O. Lépori, J.J. Silber, R.D. Falcone, N.M. Correa, Improvement of the amphiphilic properties of a dialkyl phosphate by creation of a protic ionic liquid-like surfactant, *RSC Adv.* 7 (2017) 44743–44750. <https://doi.org/10.1039/c7ra08907d>.
- [41] N. Mariano, R. Dario, Non-traditional unilamellar vesicles based on the protic ionic liquid- surfactant imim-DEHP evaluated as a function of pH and in saline, (n.d.).
- [42] W. Lin, X. Xie, Y. Yang, X. Fu, H. Liu, Y. Yang, J. Deng, Thermosensitive magnetic liposomes with doxorubicin cell-penetrating peptides conjugate for enhanced and targeted cancer therapy, *Drug Deliv.* 23 (2016) 3436–3443. <https://doi.org/10.1080/10717544.2016.1189983>.
- [43] S.A. Abraham, D.N. Waterhouse, L.D. Mayer, P.R. Cullis, T.D. Madden, M.B. Bally, The liposomal formulation of doxorubicin, *Methods Enzymol.* 391 (2005) 71–97. [https://doi.org/10.1016/S0076-6879\(05\)91004-5](https://doi.org/10.1016/S0076-6879(05)91004-5).
- [44] M. Cagel, E. Grotz, E. Bernabeu, M.A. Moretton, D.A. Chiappetta, Doxorubicin: nanotechnological overviews from bench to bedside, *Drug Discov. Today.* 22 (2017) 270–281. <https://doi.org/10.1016/j.drudis.2016.11.005>.
- [45] Z. Mirzaei-Kalar, A. Yavari, A. Jouyban, Increasing DNA binding affinity of doxorubicin by loading on Fe₃O₄ nanoparticles: A multi-spectroscopic study, *Spectrochim. Acta - Part A Mol. Biomol. Spectrosc.* 229 (2020) 117985. <https://doi.org/10.1016/j.saa.2019.117985>.
- [46] F.M. Agazzi, R.D. Falcone, J.J. Silber, N.M. Correa, Solvent Blends Can Control Cationic Reversed Micellar Interdroplet Interactions. The Effect of n- Heptane: Benzene Mixture on BHDC Reversed Micellar Interfacial Properties: Droplet Sizes and Micropolarity, *J. Phys. Chem. B.* 115 (2011) 12076–12084. <https://doi.org/10.1021/jp203014j>.
- [47] P.A. Hassan, S. Rana, G. Verma, Making sense of Brownian motion: Colloid characterization by dynamic light scattering, *Langmuir.* 31 (2015) 3–12. <https://doi.org/10.1021/la501789z>.
- [48] M. Abbas, M. Takahashi, C. Kim, Facile sonochemical synthesis of high-moment magnetite (Fe₃O₄) nanocube, *J. Nanoparticle Res.* 15 (2012) 1–12.
- [49] L. Shen, Y. Qiao, Y. Guo, S. Meng, G. Yang, M. Wu, J. Zhao, Facile co-precipitation synthesis of shape-controlled magnetite nanoparticles, *Ceram. Int.* 40 (2014) 1519–1524. <https://doi.org/10.1016/j.ceramint.2013.07.037>.
- [50] S. Akhter, D.P. Paul, M.A. Hakim, D.K. Saha, M. Al-Mamun, A. Parveen, Synthesis, Structural and Physical Properties of Cu_xZn_yFe_zO₄ Ferrites, *Mater. Sci. Appl.* 02 (2011) 1675–1681. <https://doi.org/10.4236/msa.2011.211223>.
- [51] Z. Fülöp, R. Gref, T. Loftsson, A permeation method for detection of self-aggregation of doxorubicin in aqueous environment, *Int. J. Pharm.* 454 (2013) 559–561. <https://doi.org/10.1016/j.ijpharm.2013.06.058>.
- [52] Q.Z. Wang, X.G. Chen, N. Liu, S.X. Wang, C.S. Liu, X.H. Meng, C.G. Liu, Protonation constants of chitosan with different molecular weight and degree of deacetylation, *Carbohydr. Polym.* 65 (2006) 194–201. <https://doi.org/10.1016/j.carbpol.2006.01.001>.
- [53] V. Guarino, R. Altobelli, L. Ambrosio, Chitosan microgels and nanoparticles via electrofluidodynamic techniques for biomedical applications, *Gels.* 2 (2016). <https://doi.org/10.3390/gels2010002>.
- [54] P. Parris, I. Rago, L. Ulloa Severino, F. Perissinotto, E. Ambrosetti, P. Paoletti, M. Ricci, A.P. Beltrami, D. Cesselli, L. Casalis, Atomic force microscopy analysis of extracellular vesicles, *Eur. Biophys. J.* 46 (2017) 813–820. <https://doi.org/10.1007/s00249-017-1252-4>.
- [55] N. Sebaihi, B. De Boeck, Y. Yuana, R. Nieuwland, J. Pétry, Dimensional characterization of extracellular vesicles using atomic force microscopy, *Meas. Sci. Technol.* 28 (2017). <https://doi.org/10.1088/1361-6501/28/3/034006>.
- [56] M. Skliar, V.S. Chernyshev, Imaging of extracellular vesicles by atomic force microscopy, *J. Vis. Exp.* 2019 (2019) 1–13. <https://doi.org/10.3791/59254>.
- [57] M.L. Kabir, F. Wang, A.H.A. Clayton, Red-edge excitation shift spectroscopy (Rees): Application to hidden bound states of ligands in protein–ligand complexes, *Int. J. Mol. Sci.* 22 (2021) 1–22. <https://doi.org/10.3390/ijms22052582>.
- [58] N.S. White, R.J. Errington, Fluorescence techniques for drug delivery research: Theory and practice, *Adv. Drug Deliv. Rev.* 57 (2005) 17–42. <https://doi.org/10.1016/j.addr.2004.08.003>.
- [59] C. Albrecht, Joseph R. Lakowicz: Principles of fluorescence spectroscopy, 3rd Edition, *Anal. Bioanal. Chem.* 390 (2008)

- 1223–1224. <https://doi.org/10.1007/s00216-007-1822-x>.
- [60] J. Liang, Z. Zhang, H. Zhao, S. Wan, X. Zhai, J. Zhou, R. Liang, Q. Deng, Y. Wu, G. Lin, Simple and rapid monitoring of doxorubicin using streptavidin-modified microparticle-based time-resolved fluorescence immunoassay, *RSC Adv.* 8 (2018) 15621–15631. <https://doi.org/10.1039/c8ra01807c>.
- [61] B. Gnpareddy, S. Reddy Dugasani, T. Ha, B. Paulson, T. Hwang, T. Kim, J. Hoon Kim, K. Oh, S.H. Park, Chemical and Physical Characteristics of Doxorubicin Hydrochloride Drug-Doped Salmon DNA Thin Films, *Sci. Rep.* 5 (2015) 1–9. <https://doi.org/10.1038/srep12722>.
- [62] G.A. Hussein, S. Kanan, M. Al-Sayah, Investigating the fluorescence quenching of doxorubicin in folic acid solutions and its relation to ligand-targeted nanocarriers, *J. Nanosci. Nanotechnol.* 16 (2016) 1410–1414. <https://doi.org/10.1166/jnn.2016.10700>.
- [63] M.L. Torgersen, P.J. Judge, J.F. Bada Juarez, A.D. Pandya, M. Fusser, C.W. Davies, M.K. Maciejewska, D.J. Yin, G.M. Maelandsmo, T. Skotland, A. Watts, K. Sandvig, Physicochemical Characterization, Toxicity and In Vivo Biodistribution Studies of a Discoidal, Lipid-Based Drug Delivery Vehicle: Lipodisq Nanoparticles Containing Doxorubicin, *J. Biomed. Nanotechnol.* 16 (2020) 419–431. <https://doi.org/10.1166/jbn.2020.2911>.
- [64] N.S.H. Motlagh, P. Parvin, F. Ghasemi, F. Atyabi, Fluorescence properties of several chemotherapy drugs: doxorubicin, paclitaxel and bleomycin, *Biomed. Opt. Express.* 7 (2016) 2400. <https://doi.org/10.1364/boe.7.002400>.
- [65] F. Moyano, J.J. Silber, N.M. Correa, On the investigation of the bilayer functionalities of 1,2-di-oleoyl-sn-glycero-3-phosphatidylcholine (DOPC) large unilamellar vesicles using cationic hemicyanines as optical probes: A wavelength-selective fluorescence approach, *J. Colloid Interface Sci.* (2008). <https://doi.org/10.1016/j.jcis.2007.09.051>.
- [66] D. Ray, B.K. Paul, N. Guchhait, Effect of biological confinement on the photophysics and dynamics of a proton-transfer phototautomer: An exploration of excitation and emission wavelength-dependent photophysics of the protein-bound drug, *Phys. Chem. Chem. Phys.* 14 (2012) 12182–12192. <https://doi.org/10.1039/c2cp41292f>.
- [67] H. Mishra, D. Pant, T.C. Pant, H.B. Tripathi, Edge excitation red shift and energy migration in quinine bisulphate dication, *J. Photochem. Photobiol. A Chem.* 177 (2006) 197–204. <https://doi.org/10.1016/j.jphotochem.2005.05.026>.
- [68] P. Mishra, S.K. Jha, Slow Motion Protein Dance Visualized Using Red-Edge Excitation Shift of a Buried Fluorophore, *J. Phys. Chem. B.* 123 (2019) 1256–1264. <https://doi.org/10.1021/acs.jpcc.8b11151>.
- [69] D.A.M. Catici, H.E. Amos, Y. Yang, J.M.H. van den Elsen, C.R. Pudney, The red edge excitation shift phenomenon can be used to unmask protein structural ensembles: implications for NEMO–ubiquitin interactions, *FEBS J.* 283 (2016) 2272–2284. <https://doi.org/10.1111/febs.13724>.
- [70] J.C. Kwok, D.R. Richardson, Unexpected Anthracycline-Mediated Alterations in Iron-Regulatory Protein-RNA-Binding Activity: The Iron and Copper Complexes of Anthracyclines Decrease RNA-Binding Activity, *Mol. Pharmacol.* 62 (2002) 888 LP – 900. <https://doi.org/10.1124/mol.62.4.888>.
- [71] A. Bhatta, G. Krishnamoorthy, N. Marimuthu, A. Dihingia, P. Manna, H.T. Biswal, M. Das, G. Krishnamoorthy, Chlorin e6 decorated doxorubicin encapsulated chitosan nanoparticles for photo-controlled cancer drug delivery, *Int. J. Biol. Macromol.* 136 (2019) 951–961. <https://doi.org/10.1016/j.ijbiomac.2019.06.127>.
- [72] G. Unsoy, R. Khodadust, S. Yalcin, P. Mutlu, U. Gunduz, Synthesis of Doxorubicin loaded magnetic chitosan nanoparticles for pH responsive targeted drug delivery, *Eur. J. Pharm. Sci.* 62 (2014) 243–250. <https://doi.org/10.1016/j.ejps.2014.05.021>.
- [73] G.G. Pircalabioru, C. Bleotu, C. Curutiu, G. Mihaescu, M.-C. Chifiriuc, Nanodrug delivery systems in cancer, Elsevier Inc., 2019. <https://doi.org/10.1016/b978-0-12-816506-5.00015-2>.
- [74] A. Savaser, O. Esim, S. Kurbanoglu, S.A. Ozkan, Y. Ozkan, Current perspectives on drug release studies from polymeric nanoparticles, Elsevier Inc., 2018. <https://doi.org/10.1016/B978-0-12-813663-8.00003-8>.
- [75] J. Li, S. Ying, H. Ren, J. Dai, L. Zhang, L. Liang, Q. Wang, Q. Shen, J.W. Shen, Molecular dynamics study on the encapsulation and release of anti-cancer drug doxorubicin by chitosan, *Int. J. Pharm.* 580 (2020) 119241. <https://doi.org/10.1016/j.ijpharm.2020.119241>.
- [76] J.A. Jennings, Controlling chitosan degradation properties in vitro and in vivo, Elsevier, 2017. <https://doi.org/10.1016/B978-0-08-100230-8.00007-8>.
- [77] B. Martini, S. Dimida, E. De Benedetto, M. Madaghiele, C. Demitri, Study on the degradation of chitosan slurries, *Results Phys.* 6 (2016) 728–729. <https://doi.org/10.1016/j.rinp.2016.10.012>.
- [78] X. Xu, R. Sutak, D.R. Richardson, Iron chelation by clinically relevant anthracyclines: Alteration in expression of iron-regulated genes and atypical changes in intracellular iron distribution and trafficking, *Mol. Pharmacol.* 73 (2008) 833–844. <https://doi.org/10.1124/mol.107.041335>.
- [79] X. Xu, H.L. Persson, D.R. Richardson, Molecular pharmacology of the interaction of anthracyclines with iron, *Mol. Pharmacol.* 68 (2005) 261–271. <https://doi.org/10.1124/mol.105.013383>.
- [80] A. Eizaguirre, M. Yáñez, L.A. Eriksson, Stability and iron coordination in DNA adducts of Anthracycline based anti-cancer drugs, *Phys. Chem. Chem. Phys.* 14 (2012) 12505–12514. <https://doi.org/10.1039/c2cp40931c>.
- [81] E. Munnier, S. Cohen-Jonathan, C. Linassier, L. Douziech-Eyrolles, H. Marchais, M. Soucé, K. Hervé, P. Dubois, I. Chourpa, Novel method of doxorubicin-SPION reversible association for magnetic drug targeting, *Int. J. Pharm.* 363 (2008) 170–176. <https://doi.org/10.1016/j.ijpharm.2008.07.006>.
- [82] N. Malekjani, S.M. Jafari, Modeling the release of food bioactive ingredients from carriers/nanocarriers by the empirical, semiempirical, and mechanistic models, *Compr. Rev. Food Sci. Food Saf.* 20 (2021) 3–47. <https://doi.org/10.1111/1541-4337.12660>.
- [83] M.L. Bruschi, Strategies to modify the drug release from pharmaceutical systems / edited by Marcos Luciano Bruschi., Woodhead Publishing is an imprint of Elsevier, Cambridge, UK, 2015.
- [84] E. Szymańska, K. Winnicka, Stability of chitosan - A challenge for pharmaceutical and biomedical applications, *Mar. Drugs.* 13 (2015) 1819–1846. <https://doi.org/10.3390/md13041819>.
- [85] C. Yang, X. Xing, Z. Li, S. Zhang, polymers A Comprehensive Review on Water Diffusion in Polymers Focusing on the Polymer – Metal, *Polymers.* 12 (2020) 1–27.